



# Investigating the magnetic domain structure and photonic characters of singled phased hard ferromagnetic ferrite $MFe_3O_4$ ( $M= Co^{2+}, Zn^{2+}, Cd^{2+}$ ) compounds

A. A. Ibiyemi<sup>a,\*</sup>, G. T. Yusuf<sup>c</sup>, O. Akirinola<sup>b</sup>, S. Olaniyan<sup>a</sup>, M. Orojo<sup>a</sup>, B. Osuporu<sup>a</sup>, J. Lawal<sup>d</sup>

<sup>a</sup>Department of Physics, Federal University, Oye-Ekiti, Nigeria

<sup>b</sup>Department of Physics, Ladoke Akintola University of Technology, Ogbomoso, Nigeria

<sup>c</sup>Department of Science Laboratory Technology, Osun State Polytechnic, Iree, Nigeria

<sup>d</sup>Department of Science Laboratory Technology, Federal Polytechnic, Ede, Nigeria

## Abstract

The impact of transition metals on ferrite (iron (III) oxide) compounds is investigated in this study. Ferrite samples were synthesized using the co-precipitation method. X-ray analysis unveiled the presence of the Fe-phase in the trivalent state, showcasing a single-phased cubic spinel framework with a preferred orientation along the (311) reflection plane. Crystallite sizes were determined for  $CdFe_3O_4$ ,  $ZnFe_3O_4$ , and  $CoFe_3O_4$  utilizing the Scherer equation, yielding values of 10.54 nm, 18.76 nm, and 32.63 nm, respectively. Zinc ferrite displayed an intermediate photonic nature compared to cobalt and cadmium ferrite, with cadmium ferrite showing high optical losses and cobalt ferrite exhibiting minimal optical losses. EDX analysis confirmed the presence of  $Zn^{2+}$ ,  $Co^{2+}$ ,  $Fe^{3+}$ ,  $Cd^{2+}$ , and  $O^{2-}$  ions in the correct ratios, supporting the intended stoichiometric composition. Optical assessment revealed that  $CoFe_3O_4$  nanoparticles are well-suited for optoelectronic devices, ultraviolet detectors, and infrared (IR) detectors. VSM measurements of cobalt ferrite exhibited higher coercivity and magnetic saturation compared to other samples. Photoluminescence (PL) spectroscopy revealed multiple colors, including cyan, green, and yellow, at different wavelengths for the ferrite samples. These findings suggest that the synthesized samples are suitable materials for high-frequency devices owing to their robust magnetic properties. Cadmium ferrite displayed a multi-magnetic domain structure, contrasting with the single-magnetic domain structure observed in zinc and cobalt ferrite.

DOI:10.46481/jnpsps.2024.1909

**Keywords:** Luminescence, Coercivity, Trivalent, Magnetization, Ferrite, Morphology

## Article History :

Received: 19 November 2023

Received in revised form: 17 January 2024

Accepted for publication: 19 January 2024

Published: 18 February 2024

© 2024 The Author(s). Published by the Nigerian Society of Physical Sciences under the terms of the Creative Commons Attribution 4.0 International license. Further distribution of this work must maintain attribution to the author(s) and the published article's title, journal citation, and DOI.

Communicated by: C. A. Onate

## 1. Introduction

Ferrites are magnetic materials with combined magnetic and electrical properties. Iron oxide and metal oxides are the

main components of ferrites. These cubic spinel-structured transition metal oxides have found widespread use in many technological applications during the last ten years. A significant class of semiconductors with applications in solar energy are transition metal oxides. Examples of ferrite applications include catalysis, magnetic storage, and electronics devices [1, 2].

\*Corresponding Author Tel.: +2348062198624.

Email address: [abideen.ibiyemi@fuoye.edu.ng](mailto:abideen.ibiyemi@fuoye.edu.ng) (A. A. Ibiyemi)

A trace amount of  $\text{Co}^{2+}$  ions travel from the tetrahedral A site to the octahedral B location in cobalt ferrite, an inverse ferromagnetic spinel. The presence of zinc and cadmium ions in ferrites has a major effect on the magnetic properties of ferro-spinels [3]. Cadmium ferrite ( $\text{CdFe}_2\text{O}_4$ ) is a concern because it is used in a variety of industries. Cadmium ferrites, classified as antiferromagnetic materials because cadmium ions occupy the tetrahedral positions in them, are thought to represent a typical spinel structure [4]. Cadmium-replaced ferrites show n-type semiconductor behavior, and the Seebeck coefficient steadily decreases as the cadmium content rises [5].

Cadmium ferrite has garnered interesting attention recently due to its wide range of applications in a number of scientific and engineering fields [6, 7]. Bulk cadmium ferrite is an antiferromagnetic material because  $\text{Cd}^{2+}$  ions prefer to occupy tetrahedral sites-A [8, 9]. Similar to this, ferrites substituted with  $\text{Cd}^{2+}$  ions function as n-type semiconductors, and their Seebeck value progressively decreases as the concentration of  $\text{Cd}^{2+}$  ions increases. According to a study on the application of  $\text{Cd}^{2+}$  ions in lithium ferrite, a material with high permeability, the lattice parameter rose as the amount of  $\text{Cd}^{2+}$  ions did [10]. According to ul-Islam *et al.*'s study, cadmium ferrite was predicted to have the role of a microwave field attenuator, particularly in radiative environments [11]. According to Gillot *et al.*, as the concentration of  $\text{Cd}^{2+}$  ions in cadmium ferrite rises, there is a reduction in the quantity of absorption bands [12]. Shelar *et al.* state that as the  $\text{Cd}^{2+}$  ion content rises, so does the saturation magnetization of cadmium nickel ferrite. Microwave devices benefit from the high coercivity and saturation magnetization of Cd-Ni ferrite [13]. Ni-Cd ferrite is soft magnetic and has core applications in antenna rods, recording heads, power transformer core material, and loading coils because of its high electrical resistivity and low eddy current losses, according to Viswanathan *et al.* [14]. By altering the  $\text{Cd}^{2+}$ ,  $\text{Ni}^{2+}$ , and  $\text{Fe}^{3+}$  cation composition of the unit cell, one can readily change the optical, structural, and magnetic properties of Cd-Ni ferrite. Doping Ni-ferrite with non-magnetic ions, like  $\text{Cd}^{2+}$ , causes increased saturation magnetization and decreased magnetic coupling of Cd-Ni ferrite nanomagnetic particles [14].

Transition metal ferrite nanoparticles have garnered a lot of attention lately due to their unique properties that enable them to be used in fields such as magnetic storage, biomedicine, ferrofluids, catalysis, and magnetic refrigeration systems [15–18]. Among them is zinc ferrite, which has a high electric resistance and a low eddy current loss. This particular ferrite exhibits remarkable properties such as ferromagnetism, excellent heat conductivity, strong resistance to electrical current, regulated saturation magnetization, efficient energy transmission, modest thermal expansion coefficients efficiency in ferromagnetic resonance, short line width, and strong resilience to radiation damage [19–22]. It also has unique mechanical, electrical, thermal, and magneto-optical properties. Zinc ferrite has these properties, which make it useful for a variety of applications in electrical, magnetic, sensors, battery anode, catalyst, laser, microwave, and electrochemical devices.

Methodological significance dictates that the high magnetism, high permeability, and high electrical resistivity of

spinel ferrites depend on the kind of ions present, how charged they are, and how evenly distributed they are among the tetrahedral and octahedral sites. Due to the special magnetic properties of ferrite, which make it perfect for high-frequency applications, scientists have been developing new ferrite compositions with these desired characteristics. These compositions have been utilized to manufacture a variety of electromagnetic devices [23, 24]. Since spinel of type  $\text{A}^{2+}\text{B}_2^{3+}\text{O}_4$  has drawn significant attention in a number of technological fields [25], cobalt ferrite is one of the possible candidates for magnetic and magneto-optical recording media [26–29]. Here, A and B stand for the tetrahedral and octahedral sites in the oxygen lattice, respectively.  $\text{Zn}^{2+}$  ions are found in tetrahedral positions and  $\text{Fe}^{3+}$  ions are found in octahedral sites in  $\text{ZnFe}_2\text{O}_4$ , a typical spinel structure. While  $\text{CoFe}_2\text{O}_4$  has an inverted spinel structure with  $\text{Fe}^{3+}$  ions equally distributed between tetrahedral and octahedral sites and  $\text{Co}^{2+}$  ions in octahedral sites,  $\text{ZnFe}_2\text{O}_4$  has been found to have the most intriguing morphological, structural, and magnetic features to investigate [30]. Therefore, Zn substitution in  $\text{CoFe}_2\text{O}_4$  may result in some deformed spinel structures.

The impact of the redistribution of cations ( $\text{Cd}^{2+}$ ,  $\text{Zn}^{2+}$ , and  $\text{Co}^{2+}$ ) when they are sandwiched into a ferrite ( $\text{Fe}_3\text{O}_4$ ) lattice is the appropriate focus of this study. The co-precipitation technique is used to replace  $\text{M}^{2+}$  ( $\text{M}^{2+} = \text{Cd}^{2+}$ ,  $\text{Zn}^{2+}$ , and  $\text{Co}^{2+}$ ) ions in the  $\text{MFe}_3\text{O}_4$  lattice. The  $\text{MFe}_3\text{O}_4$  lattice's optical, magnetic, luminescence, structural, and surface morphology characteristics were investigated for every  $\text{M}^{2+}$  ion replacement ( $\text{M}^{2+} = \text{Cd}^{2+}$ ,  $\text{Zn}^{2+}$ , and  $\text{Co}^{2+}$ ). Future uses of bivalent transition metals doped with trivalent nano ferrites and the study of their developing magnetically active ferrite properties are important aspects of this work. These include transition metal complexes of bivalent metal oxides, such as zinc (Zn(II)), cadmium (Cd(II)), and cobalt (Co(II)). Vibrational Sample Magnetometer (VSM), photoluminescence (PL), Energy Dispersive Spectroscopy (EDX), and X-ray diffractometer (XRD) are used to characterize the nano ferrites in great detail. Scanning Electron Microscopy (SEM) is used to analyze the surface morphology of the nano ferrites. The presence of ferrite nanoparticles in cubic spinel is explained by these findings.

## 2. Methodology

Before synthesizing the ferrite samples, deionized water, detergent, isopropyl ethanol, and acetone were used to thoroughly clean the beakers. To remove any contaminants, the beakers underwent a thorough cleaning. Using the co-precipitation technique, zinc ferrite sample is formed by the mixture of zinc (II) chloride hexahydrate ( $\text{ZnCl}_2 \cdot 6\text{H}_2\text{O}$ ) and anhydrous iron (III) chloride ( $\text{FeCl}_3$ ). Cobalt ferrite sample was synthesized by mixing cobalt chloride hexahydrate [ $\text{CoCl}_2 \cdot 6\text{H}_2\text{O}$ ], and iron chloride hexahydrate [ $\text{FeCl}_3 \cdot 6\text{H}_2\text{O}$ ] while cadmium ferrite sample was synthesized by the mixture of anhydrous cadmium nitrate tetrahydrate  $\text{Cd}(\text{NO}_3)_2 \cdot 4\text{H}_2\text{O}$  and anhydrous iron (III) chloride ( $\text{FeCl}_3$ ). are the initial reagents. Using a digital weighing balance, the weight of the

necessary quantity of aqueous solutions was ascertained. In appropriate stoichiometric ratios, zinc, cadmium, cobalt, and iron chlorides were added and dissolved in deionized water for respective ferrite components. Using a magnetic stirrer, we first dissolved aqueous solutions of cobalt chloride, and iron chloride in 500 milliliters of deionized water. We then heated each solution separately for 25 minutes at 60 degrees Celsius to create a homogenous mixture. To obtain precipitate, ammonia was added in drops until a pH of 11 was reached. Sodium hydroxide was also added to stabilize the pH. The resulting nanoparticles were dried on a hot plate, magnetically decanted, and cleaned with deionized water to get rid of extraneous particles. The samples were dried, and then grinded into fine granules using mortar. Same procedures were followed in synthesizing cadmium ferrite and zinc ferrite.

Using a UV-VIS-IR spectrophotometer, the optical characteristics of the nanomagnetic samples, such as transmittance and absorbance, were investigated. A scanning electron microscope (Jeol equipment) was used to study the surface morphology. Using an X-ray diffraction technique (Rigaku powder X-ray Diffractometer Ruker Advanced D8 model with  $\text{CuK}\alpha$  radiation,  $\lambda = 1.5406 \text{ \AA}$ ), the structural characteristics were investigated. Energy Dispersive X-ray Spectroscopy (Quantax 200 with X Flash e Bruker) was used to form the atomic composition. A photoluminescence (PL) spectrometer (FLS 100) was used to analyze the light luminescence. The Vibrating Sample Magnetometer (VSM) was used to estimate the magnetic behaviors.

### 3. Results and Discussion

#### 3.1. Compositional Analysis of $M\text{Fe}_3\text{O}_4$ ( $M = \text{Zn}^{2+}, \text{Cd}^{2+}, \text{Co}^{2+}$ ) magnetic samples

The elemental makeup of the generated compounds was ascertained using Elemental Dispersive X-ray Spectroscopy (EDS). The EDS spectrum of the synthesized ferrite compounds is displayed in Figure 1. The appropriate stoichiometry and the EDS data agree fairly well. The EDS spectra showed the formation of particles of cobalt (Co), zinc (Zn), cadmium (Cd), iron (Fe), and oxygen (O), as well as the presence of impurities such as nitrogen (N), sulphur (S), gold (Au), and chlorine (Cl). The existence of  $\text{Cl}^-$  may result from partial substitution of  $\text{Cl}^-$  particles into the  $\text{Fe}^{3+}$  lattice site during synthesis, while incomplete oxidation of  $\text{Cd}(\text{NO}_3)_2$  may be the cause of  $\text{N}^{2-}$ . It was discovered that the generated  $\text{CdFe}_3\text{O}_4$  nanomagnetic compounds contained about 8% impurities. The authors are uncertain about the origin of the gold particle (Au) synthesis, which is restricted to  $\text{CdFe}_2\text{O}_4$  nanomagnetic particles, as can be seen in Figure 1a.

#### 3.2. Optoelectronics and Photonics analysis of the Synthesized Samples

##### 3.2.1. Optical Energy Band Gap of $M\text{Fe}_3\text{O}_4$ ( $M = \text{Cd}^{2+}, \text{Co}^{2+}, \text{Zn}^{2+}$ ) Magnetic Samples

Plotting photon energy ( $h\nu$ ) against  $[\text{F}(r)h\nu]^2$  allowed researchers to determine the optical energy band gap of the fer-

rite samples using the Diffuse Reflection Spectroscopy (DRS) technique.

The Kubelka-Munk function  $F(r)$  is given by

$$F(r) = k/S,$$

where  $k$  = molar absorption coefficient and  $S$  is the scattering factor.

$S$  is the scattering factor which is given as  $2R$ .

The molar absorption coefficient  $k$  is given in equation (1);

$$k = (1 - R)^2, \quad (1)$$

where  $R$  is the reflectance.

As seen in Figure 2, the energy band gap is found by extrapolating the spectra lines' linear course. The energy band gap ranged between 2.78 and 3.65 eV, indicating that the band gap changes as a bivalent cationic metal sandwiched into trivalent ferrite sites changed. According to reports, ferrite (iron oxide) has an energy band gap of 2.2 eV [31], but its physical state changes when metallic ions like  $\text{Cd}^{2+}$ ,  $\text{Zn}^{2+}$ , and  $\text{Co}^{2+}$  are sandwiched into it. When the bivalent cationic metals in ferrite is replaced, the cations are redistributed on tetrahedral site-A and octahedral site-B, resulting in a change in energy band gap [32–35].

The linear course of the spectra lines is extrapolated to find the energy band gap, as shown in Figure 2. The energy band gap varied from 2.78 to 3.65 eV, indicating that the band gap changes as a bivalent cationic metal sandwiched into trivalent ferrite sites changed. The energy band gap 3.65 eV favorably match with result reported by Anjum *et al.* [35] for cobalt ferrite. Ferrite, or iron oxide, is said to have an energy band gap of 2.2 eV as reported by [31], but when metallic ions such as  $\text{Cd}^{2+}$ ,  $\text{Zn}^{2+}$ , and  $\text{Co}^{2+}$  are sandwiched into it, its physical state is altered. The cations are redistributed on tetrahedral site-A and octahedral site-B upon replacement of the bivalent cationic metals in ferrite, causing a shift in the energy band gap.

Synthesizing a cobalt ferrite sample results in a very high band gap of approximately 3.65 eV, which is sufficient to cause a significant physical change in the ferrite's optical state. The optical capacity of the  $\text{CdFe}_2\text{O}_4$  nanoparticle with a band gap of 2.68 eV is limited because only photons below a threshold wavelength  $\lambda_g$  may be absorbed because the solar spectrum reaches its maximum intensity at approximately 2.7 eV [36]. On the other hand, the band gap for  $M\text{Fe}_2\text{O}_4$  is measured to be 2.68 eV at  $M = \text{Cd}^{2+}$  and 3.05 eV at  $M = \text{Zn}^{2+}$ . As a result, quantum-sized particles were produced at  $M = \text{Cd}^{2+}$  in  $M\text{Fe}_3\text{O}_4$ , which show the band gaps whose photons fall inside the threshold wavelength  $\lambda_g$  for light absorption. The structural zone model for polycrystalline metallic samples similarly explains these observations. Crystallite diameters shrank as a result of segregation at grain boundaries brought on by changing of cationic metals in ferrite lattice sites [37]. In light of this, the ideal spinel of  $M\text{Fe}_2\text{O}_4$  may be found at 3.65 eV, which would result in the highest-quality crystalline nanoparticles. The conclusions concur with those of Suman *et al.* [38] and Nikolai *et al.* [39]. While the Fermi level shifts close to the conduction band due to an increase in carrier concentration, the low energy

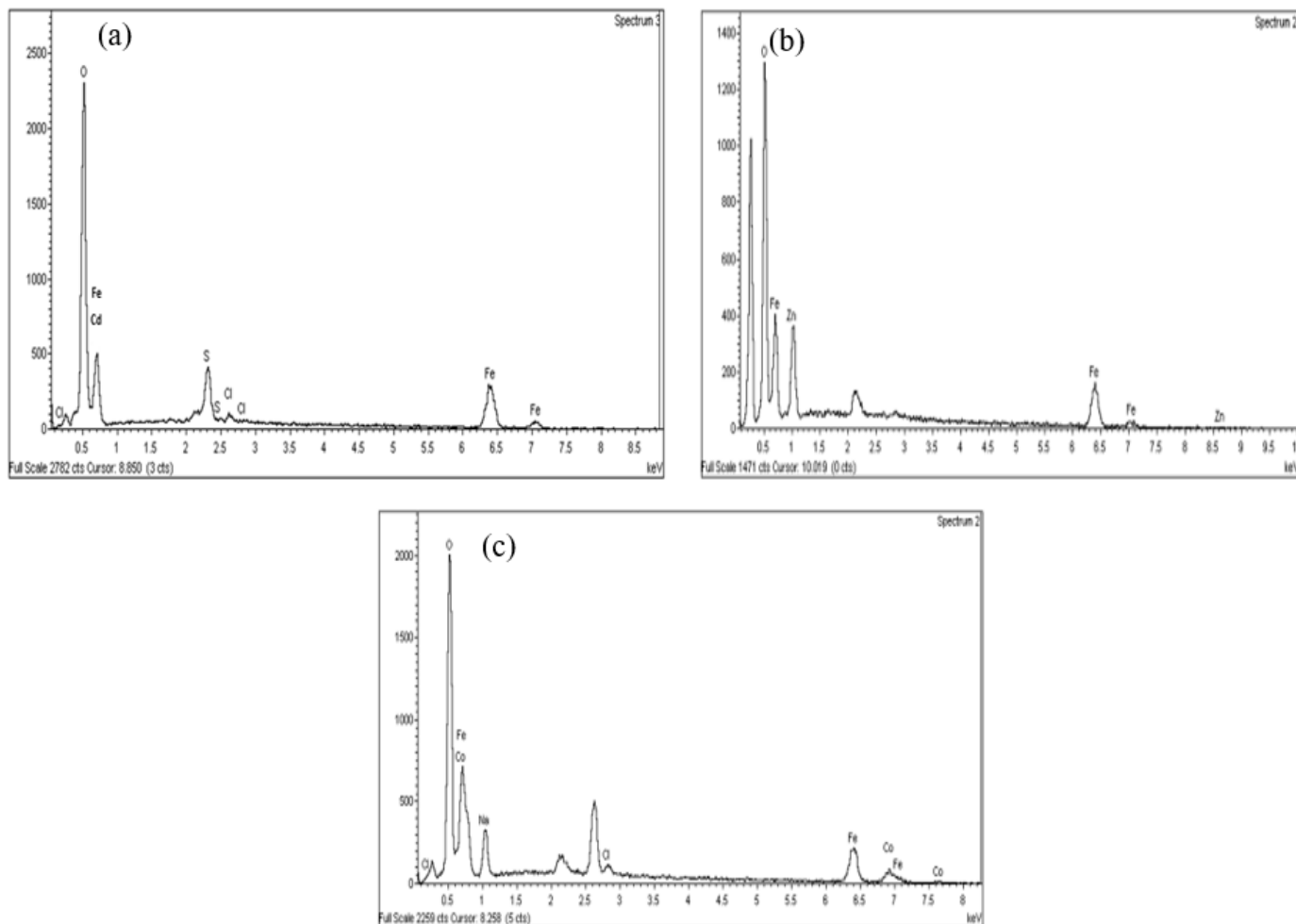


Figure 1. EDS spectral of (a)  $MFe_3O_4$  ( $M = Cd^{2+}$ ) magnetic sample, (b)  $MFe_3O_4$  ( $M = Zn^{2+}$ ) magnetic sample (c)  $MFe_3O_4$  ( $M = Co^{2+}$ ) magnetic sample.

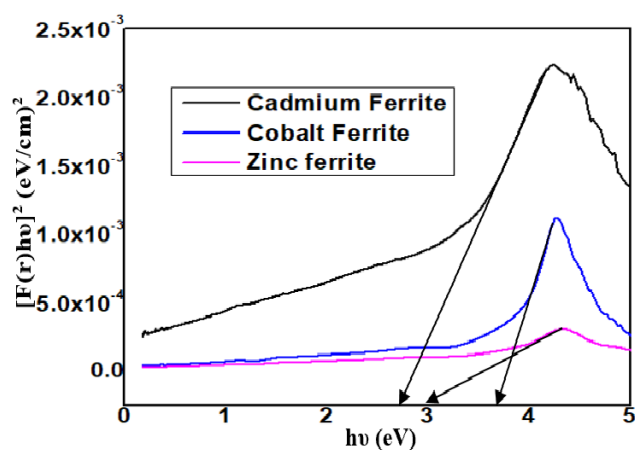


Figure 2. Optical energy band gap spectral of  $MFe_3O_4$  ( $M = Cd^{2+}$ ,  $Co^{2+}$ ,  $Zn^{2+}$ ) magnetic samples.

transition is blocked and the band gap increases due to cationic metals substitution in the ferrite lattice, the increase in band

gap from 2.68 eV to 3.65 eV for  $M = Cd^{2+}$ ,  $Zn^{2+}$  and  $Co^{2+}$  in that order, also known as the blue shift, can be explained based on the Burstein-Moss effect [40]. It is evident from the energy band gap values that the nanoparticles have a wide range of optoelectronic applications, especially when used as window layers in solar cells.

### 3.2.2. Optical Transmittance of $MFe_3O_4$ ( $M = Cd^{2+}$ , $Co^{2+}$ , $Zn^{2+}$ ) Magnetic Samples

The transmittance of  $MFe_3O_4$  particles ( $M = Cd^{2+}$ ,  $Zn^{2+}$ , and  $Co^{2+}$ ) is displayed in Figure 3. In the following order, transmittance to photon energy increases for  $M = Cd^{2+}$ ,  $Zn^{2+}$ , and  $Co^{2+}$ . The bivalent ions  $M^{2+}$  and trivalent ions  $Fe^{3+}$  ions are reallocated on the tetrahedral site-A and octahedral site-B when the component of M in  $MFe_3O_4$  is changed when cations  $M^{2+}$  ( $Cd^{2+}$ ,  $Co^{2+}$ ,  $Zn^{2+}$ ) are substituted in ferrite. The findings show that the redistribution of  $Cd^{2+}$ ,  $Zn^{2+}$ ,  $Co^{2+}$ , and  $Fe^{3+}$  ions on sites A and B alters the systemic optical function of  $MFe_3O_4$  samples. High percentage photon energy transparency is exhibited by  $CoFe_2O_4$  nanoparticles in the visible and infrared regions of the electromagnetic spectrum. A low percentage trans-

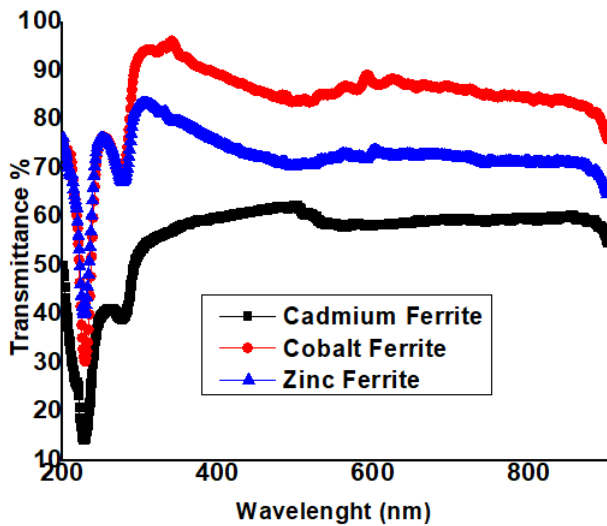


Figure 3. Optical transmittance spectral of  $MFe_3O_4$  ( $M = Cd^{2+}$ ,  $Co^{2+}$ ,  $Zn^{2+}$ ) magnetic samples.

mittance of roughly 58% is produced within the visible region when the M component of  $MFe_3O_4$  is changed to  $Cd^{2+}$ , whereas a maximum percentage transmittance of approximately 95% is formed when the  $MFe_3O_4$  sample is synthesized with  $M = Co^{2+}$ . When M is  $Cd^{2+}$ ,  $Zn^{2+}$ , or  $Co^{2+}$  in  $MFe_2O_4$ , the percentage transmittance value of each sample is 58%, 78%, and 95%, respectively, at varying M in  $MFe_2O_4$ .

The  $Co^{2+}$  ion composition exhibits enhanced transmittance because it increases the number of optical charge carriers (electrons) generated and raises the energy level in the energy band by adding new energy levels. The large number of charged particles (electron transfers) from the valence band to the conduction band in the  $MFe_2O_4$  sample produced at  $M = Co^{2+}$  also results in higher % transmittance. The synthesized  $MFe_2O_4$  sample at  $M = Co^{2+}$  can now be used to enhance window layer production for solar cell applications and is appropriate for the creation of effective optoelectronic devices. Because of its increased optical gain, another  $MFe_2O_4$  sample synthesized at  $M = Zn^{2+}$  is also well suited for optoelectronic device application, though it is less efficient than the  $MFe_2O_4$  sample synthesized at  $M = Co^{2+}$ .

Large optical loss is produced by the  $CdFe_2O_4$  sample's high optical absorption of incident photons; this could be because the material contains impurities. The  $CoFe_2O_4$  nanomagnetic particle forms low optical losses, improving optoelectronic applications. For  $M = Cd^{2+}$ ,  $Zn^{2+}$ , and  $Co^{2+}$ , respectively, the samples exhibit a similar pattern in the infrared spectrum, with percentage transmittances of roughly 53%, 70%, and 78%.  $ZnFe_2O_4$  and  $CoFe_2O_4$  magnetic samples are more transparent to infrared light, according to the findings, which means that these ferrites can now be used to create the ideal material for infrared radiation detection.

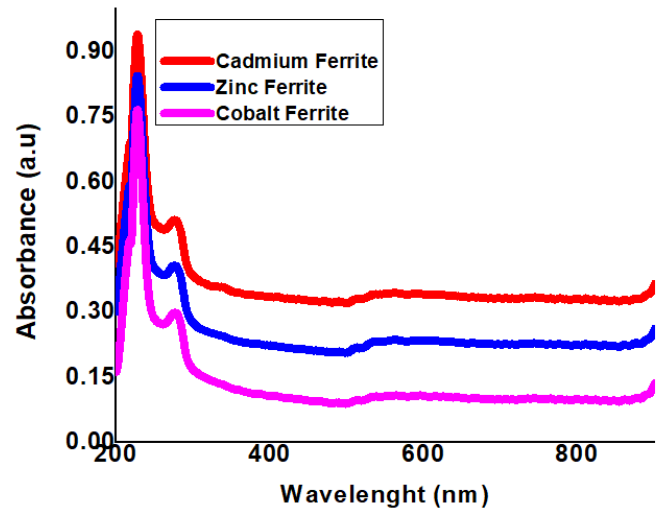


Figure 4. Optical absorbance spectral of  $MFe_3O_4$  ( $M = Cd^{2+}$ ,  $Co^{2+}$ ,  $Zn^{2+}$ ) magnetic samples.

### 3.2.3. Optical Absorbance of $MFe_3O_4$ ( $M = Cd^{2+}$ , $Co^{2+}$ , $Zn^{2+}$ ) Magnetic Samples

Figure 4 shows the absorption bands produced by  $MFe_3O_4$  ferrite magnetic nanoparticles. The center of the blue-shifted absorption edge, which is consistent with the  $MFe_3O_4$  ferrite excitonic band, is between 240 and 280 nm. Samples of  $MFe_3O_4$  ferrite showed significant absorption of UV light and produced a high absorption peak position at 240 nm. After that, this peak moved to a position close to visible light, where a weak absorption band formed at 280 nm. Weaker absorption bands were observed at 280 nm in the ultraviolet spectrum, while a strong absorption band was formed at 240 nm. The absorption band at 240 nm is due to strain brought on by the M ( $M = Cd^{2+}$ ,  $Zn^{2+}$ ,  $Co^{2+}$ ) ion entering the  $Fe^{3+}$  ion lattice, which results in a lattice defect. Each sample exhibited similar properties and showed little absorption at visible and infrared wavelengths. The results showed that  $CoFe_3O_4$  nanomagnetic particles had low absorption due to their high transmittance to photon energy.  $CoFe_2O_4$  magnetic nanoparticles have a lower absorbance than  $CdFe_2O_4$  magnetic nanoparticles, which has a higher absorbance. UV detectors can be suitably employed with  $CdFe_2O_4$  ferrite samples that exhibit increased optical absorption edge in the ultraviolet spectrum. Similar result was reported by Saleem *et al.* [32], Anjum *et al.* [35] and Arshad *et al.* [33]. From now on,  $CdFe_2O_4$  ferrite nanomagnetic sample works well for UV control in architectural windows and UV photodetector since it senses, absorbs and filters UV radiation that could cause interior home systems to heat up. This material is a better compound for effective UV radiation control due to its high absorption in the ultraviolet region.

### 3.2.4. Optical reflectance of $MFe_3O_4$ ( $M = Cd^{2+}$ , $Co^{2+}$ , $Zn^{2+}$ ) magnetic samples

Figure 5 displays the photoreflexion of  $MFe_3O_4$  samples ( $M = Cd^{2+}$ ,  $Zn^{2+}$ , and  $Co^{2+}$ ). As the component M in  $MnFe_3O_4$  is substituted, the photo-reflection of  $MFe_3O_4$  magnetic sam-

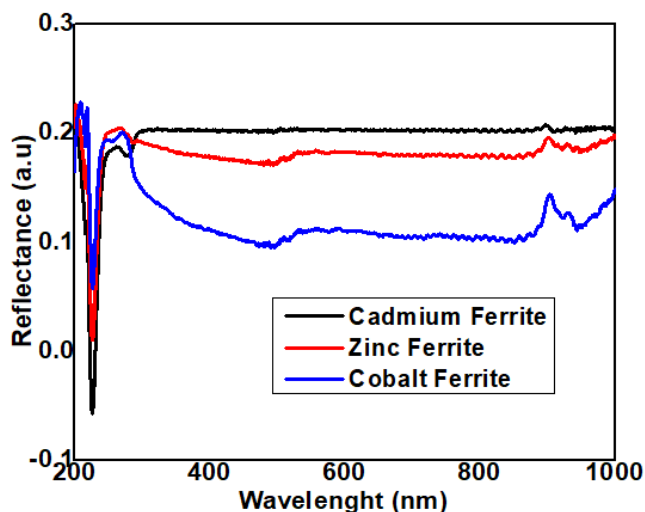


Figure 5. Optical reflectance spectral of  $MFe_3O_4$  ( $M = Cd^{2+}, Co^{2+}, Zn^{2+}$ ) magnetic samples.

ples is altered. In that order, reflectance to photon energy decreases for  $M = Cd^{2+}, Zn^{2+}$ , and  $Co^{2+}$ . The behavior of all the samples was similar:  $CdFe_3O_4$  magnetic nanoparticles displayed greater optical reflection than  $CoFe_3O_4$  magnetic samples, which displayed less optical reflection. The results show that  $CoFe_3O_4$  magnetic samples are perfect for anti-reflection device application and can be used for coating industrial devices that require minimal reflection because they isolate unwanted reflection from optical devices. When an optical device is coated with a  $CoFe_3O_4$  magnetic sample, there is little reflection of the incident photon. This material's suitability as an anti-reflection compound in basic engineering systems was demonstrated by its high transmittance, low absorbance, and low reflection to photon energy. Anti-reflection device manufacturing is challenging in optoelectronic device applications; however, coating materials containing  $CoFe_3O_4$  material reduce reflection and facilitate the creation of efficient anti-reflection devices.

### 3.2.5. Surface Morphology of $MFe_3O_4$ ( $M = Cd^{2+}, Co^{2+}, Zn^{2+}$ ) Magnetic Samples

Figure 6 displays the surface morphologies of nanomagnetic samples of  $CdFe_3O_4$ ,  $ZnFe_3O_4$ , and  $CoFe_3O_4$ . Figure 6a illustrates the formation of a fairly packed microstructure and spheroid grains with minimal porous morphology in the sample synthesized at  $M = Cd^{2+}$  in  $MFe_3O_4$ . There are visible voids and cracks in the surface framework, indicating that the surface layer is not uniform. Figure 6b shows the surface arrangement of the sample grains prepared at  $M = Zn^{2+}$  in  $MFe_3O_4$ . The surface exhibits the formation of closely spaced microstructures and spherically shaped grains. Every time  $M$  in  $MFe_3O_4$  is changed,  $MFe_3O_4$  showed the progression of structural rearrangement. Figure 6c show the surface framework of samples developed with  $M = Co^{2+}$  in  $MFe_3O_4$ . The morphology of cobalt ferrite was largely homogeneous, with spherically shaped grains. Similar result was reported by Thakur *et al.*

[41]. Even though  $CoFe_3O_4$  revealed smaller grain sizes than  $CdFe_3O_4$ ,  $CoFe_3O_4$  demonstrated the production of microstructures with a spherical shape and very little agglomeration. On the other hand, the grain agglomeration in  $CdFe_3O_4$  is more pronounced. The surface morphology of the grown  $CoFe_3O_4$  samples revealed minimal surface imperfections such as pores, holes, and cavities, and the surface organization showed the evolution of low particle aggregation. The morphologies show the appearance of a densely packed spherical microstructure and the absence of a second phase particle. Large agglomeration was seen in  $CdFe_3O_4$ , which could be the result of distortion at the lattice site and the presence of impurities. The lattice distortion could be brought on by the replacement of  $Cd^{2+}$  and  $Fe^{3+}$  ions on octahedral B-sites and tetrahedral A-sites. The substitution of  $Fe^{3+}$ , which has an ionic radius of 64 Å, for the larger  $Cd^{2+}$  ion in the B-site, which has an ionic radius of 94 Å, is what causes the lattice distortion.

### 3.2.6. X-ray Diffraction of $MFe_3O_4$ ( $M = Cd^{2+}, Co^{2+}, Zn^{2+}$ ) Magnetic Samples.

The X-ray diffraction patterns of the synthesized magnetic ferrites nanoparticles are displayed in Figure 7a-c. The trivalent state XRD data suggested the formation of the Fe phase. Similar findings have been reported by a number of researchers [42–47]. These findings support the development of the FCC framework and single phase spinel structure. The locations where the diffraction peaks formed were the reflection planes (220), (311), (222), (400), (511), (422), and (440), and the diffraction angles  $29.654^\circ$ ,  $35.125^\circ$ ,  $36.736^\circ$ ,  $41.978^\circ$ ,  $52.643^\circ$ ,  $57.043^\circ$ , and  $62.384^\circ$ . However, there is a slight variation in the diffraction angle as the  $M$  in  $MFe_3O_4$  changes. The results show that the X-ray diffraction peaks in the XRD pattern exactly match the standard pattern for that ferrite in (JCPDS No: 10-325). It was observed that the diffraction peaks were broader; this was caused by both unit cell expansion and modifications in the lattice properties. Ionic radii for  $Zn^{2+}$ ,  $Co^{2+}$ ,  $Cd^{2+}$ , and  $Fe^{3+}$  ions are 0.74 Å, 0.65 Å, 0.95 Å, and 0.64 Å, respectively [37, 39]. The lattice parameter changed as a result of competition between the  $Fe^{3+}$  ions and any of these cationic metals ( $Zn^{2+}$ ,  $Co^{2+}$ ,  $Cd^{2+}$ ) at tetrahedral sites (A) and octahedral sites (B) in the unit cell. The variation of cationic metals in ferrite affects the lattice parameter.  $CoFe_3O_4$ ,  $ZnFe_3O_4$ , and  $CdFe_3O_4$  have lattice parameters of 0.834 Å, 0.856 Å, and 0.862 Å, in that order. Because the larger ionic radii of  $Cd^{2+}$  are replaced with smaller ionic radii of  $Fe^{3+}$ ,  $CdFe_3O_4$  has the highest lattice parameter. Because the ferrite lattice is more strained when  $Fe^{3+}$  is substituted for  $Cd^{2+}$  ions in the lattice sites, the lattice parameter of  $CdFe_3O_4$  is larger. Even though the ionic radii of  $Fe^{3+}$  are smaller than those of  $Co^{2+}$  and  $Zn^{2+}$ , substituting  $Fe^{3+}$  for  $Zn^{2+}$  and  $Co^{2+}$  results in less strain on the lattice and the formation of a smaller lattice parameter. The differences in the ionic radii of the  $Cd^{2+}$ ,  $Zn^{2+}$ ,  $Co^{2+}$ , and  $Fe^{3+}$  ions account for this effect. Variations in ionic radii lead to the expansion of the unit cell because cationic metals compete with each other to occupy the same unit cell within the lattice site. A larger lattice constant was the result of an attempt to replace the smaller ionic radius of  $Fe^{3+}$  ions with the larger ionic radius of  $Cd^{2+}$  ions.

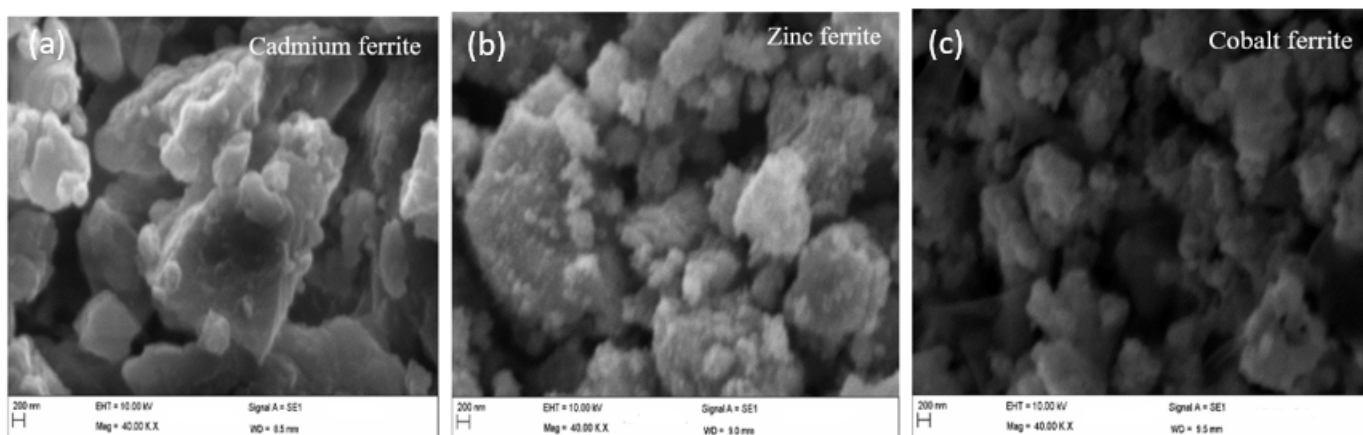


Figure 6. Surface morphological image of (a)  $\text{MFe}_3\text{O}_4$  ( $\text{M} = \text{Cd}^{2+}$ ) magnetic sample, (b)  $\text{MFe}_3\text{O}_4$  ( $\text{M} = \text{Zn}^{2+}$ ) magnetic sample, (c)  $\text{MFe}_3\text{O}_4$  ( $\text{M} = \text{Co}^{2+}$ ) magnetic sample.

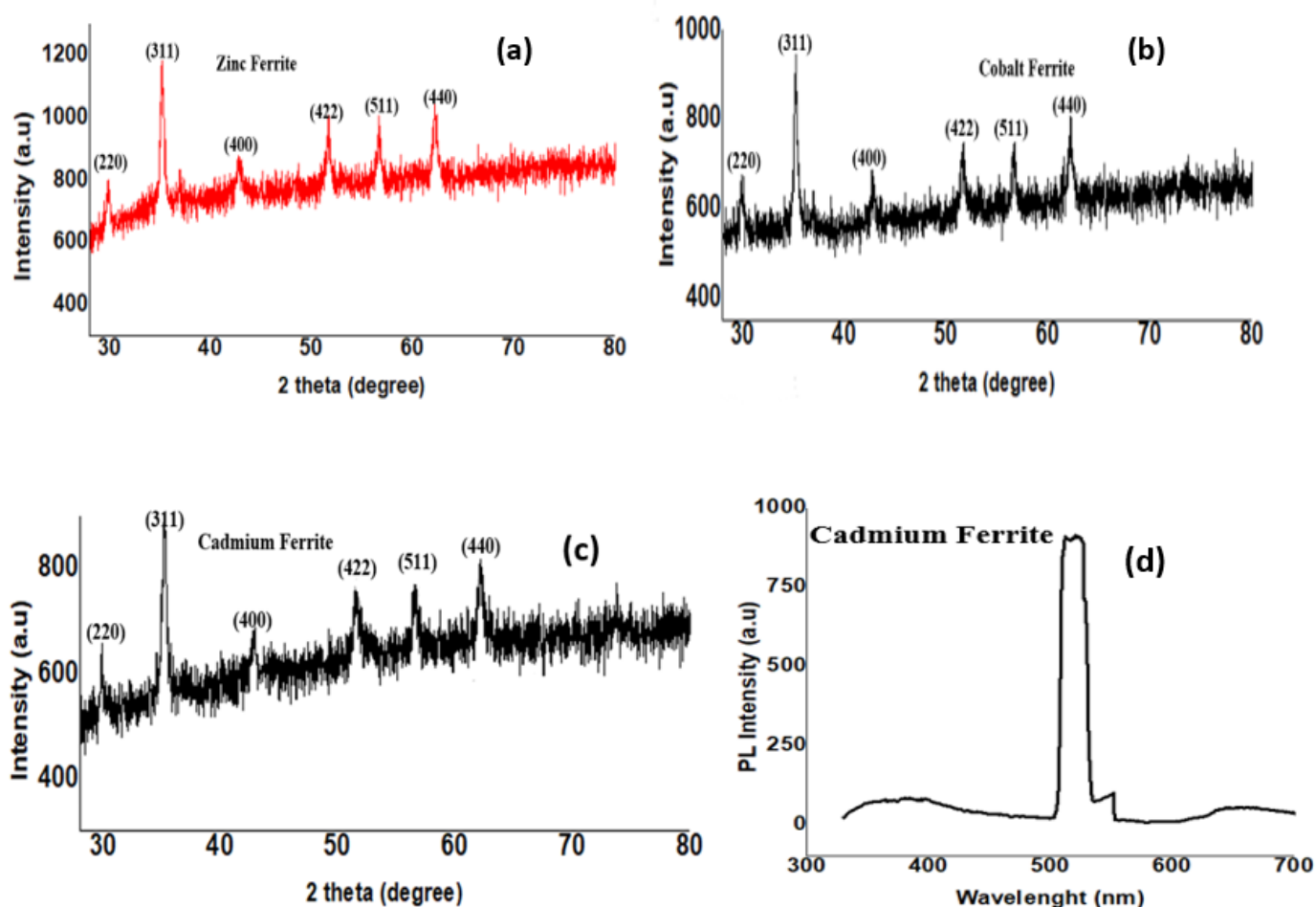


Figure 7. X-ray diffraction spectral of (a)  $\text{MFe}_3\text{O}_4$  ( $\text{M} = \text{Zn}^{2+}$ ) magnetic samples, (b)  $\text{MFe}_3\text{O}_4$  ( $\text{M} = \text{Co}^{2+}$ ) magnetic samples, (c)  $\text{MFe}_3\text{O}_4$  ( $\text{M} = \text{Cd}^{2+}$ ) magnetic samples, (d) Photoluminescence spectral of  $\text{MFe}_3\text{O}_4$  ( $\text{M} = \text{Cd}^{2+}$ ) magnetic samples

The observed slight shifting of diffraction peaks is caused by the rivalry between cationic metals for occupying tetrahedral sites (A) and octahedral sites (B), which leads to the creation of a lattice defect [44]. The formation of multiple peaks indi-

cates the presence of a polycrystalline structure. Equation (2) was used to quantify the size of the crystallites using the Derby Scherrer equation, while Equation (3) was used to calculate the lattice constant. The crystallite size as determined by Derby

Scherrer method revealed a change in the lattice site of the ferrite as the cationic ions were replaced.  $\text{Co}^{2+}$  ions sandwiched into ferrite  $\text{MFe}_3\text{O}_4$  lattice sites revealed the larger crystallite size [48, 49]

$$D = \frac{k\lambda}{\beta\cos\theta} \quad (2)$$

$$a = d\sqrt{h^2 + k^2 + l^2}, \quad (3)$$

where  $\beta$  is the complete width at half the maximum of the diffraction peak,  $\theta$  is the corresponding diffraction angle,  $D$  is the crystallite size,  $k$  is the shape factor, and  $\lambda$  is the wavelength of the x-ray. The Scherer equation was used to calculate the crystallite size, and the results revealed sizes such as 10.54 nm, 18.76 nm and 32.63 nm for  $\text{CdFe}_3\text{O}_4$ ,  $\text{ZnFe}_3\text{O}_4$  and  $\text{CoFe}_3\text{O}_4$  respectively.

### 3.2.7. Photoluminescence Analysis of $\text{MFe}_3\text{O}_4$ ( $M = \text{Cd}^{2+}$ , $\text{Co}^{2+}$ , $\text{Zn}^{2+}$ ) Magnetic Samples.

We use photoluminescence spectroscopy to investigate the luminescence effect of  $\text{MFe}_3\text{O}_4$  ferrite samples. The broadening emission bands in  $\text{MFe}_3\text{O}_4$  ferrite samples at various wavelengths are shown in Figure 8b. Broad luminescence peaks are believed to be produced by the formation of oxygen vacancies in the ferrite lattice and the presence of donor energy levels near the conduction band edge [50]. The electron transfer from the donor level to the acceptor level is responsible for the formation of a noticeable emission peak in all of the synthesized samples. Figure 8b illustrates how the  $\text{CoFe}_3\text{O}_4$  sample exhibits a broadened, narrowed emission band with a sharp edge at wavelength 550 nm where green emission is observed. Green light emitting  $\text{CoFe}_3\text{O}_4$  samples are typically designed and used as light emitting diodes. It is believed that a defect, such as oxygen vacancies, is responsible for the dramatic luminescence peak; the defect is brought about by donor levels close to the oxide's conduction band edge [51]. Figure 8a illustrates the  $\text{ZnFe}_3\text{O}_4$  sample's non-sharp luminescence peak and broadened, widening emission bands where yellow emission is visible between 560 and 590 nm. Figure 7d illustrates the non-sharp luminescence peak of the  $\text{CdFe}_3\text{O}_4$  sample as well as the broadened, widening emission bands between 510 and 530 nm, where green and cyan emission are visible at different wavelengths. The effect of particle size caused the emission bands to widen. A minor shift in the emission band is observed as a result of  $M$  being replaced in  $\text{MFe}_3\text{O}_4$ . The shift in the emission bands results from the formation of an impurity level in the  $\text{MFe}_3\text{O}_4$  ferrite lattice. The  $\text{MFe}_3\text{O}_4$  lattice's impurity level formation is what caused the emission band shifting. The formation of cyan, green, and yellow light emissions is indicated by the shifting of the peaks from a maxima energy level to a minimal energy level at 510 nm to 550 nm and 570 nm. The results show that light emission is impacted by interface defects, which are dependent on the excitation energy, particle sizes, and intensity of the incident light. The creation of deep levels in the visible region and localized levels in the energy band is attributed to the green emission [52].

### 3.2.8. Investigating the Magnetic Properties of $\text{MFe}_3\text{O}_4$ ( $M = \text{Cd}^{2+}$ , $\text{Co}^{2+}$ , $\text{Zn}^{2+}$ ) Magnetic Samples.

Using a vibrating sample magnetometer, the magnetic characteristics of  $\text{MFe}_3\text{O}_4$  ( $M = \text{Cd}^{2+}$ ,  $\text{Zn}^{2+}$ ,  $\text{Co}^{2+}$ ) magnetic samples were investigated. Plotting the applied magnetic field against magnetization allowed for the analysis of the magnetic characteristics. Table 1 contains a list of the magnetic parameter values.

The magnetic properties were examined using a vibrating sample magnetometer (VSM), and the magnetic elements—saturation magnetization ( $M_s$ ), remanence magnetization ( $M_r$ ), coercivity ( $H_c$ ), and remanence ratio—were obtained using the hysteresis curve shown in Figure 9. Based on the curve, the estimated saturation magnetization values for the  $\text{CoFe}_3\text{O}_4$ ,  $\text{CdFe}_3\text{O}_4$ , and  $\text{ZnFe}_3\text{O}_4$  samples are 64.779 emu/g, 24.041 emu/g, and 39.263 emu/g, respectively. The significant saturation magnetization may result from the crystalline nature of the  $\text{CoFe}_3\text{O}_4$  nanoparticle and the formation of a minimum surface structural defect. The high saturation magnetization of cobalt ferrite may also be due to small crystal lattice defects and low magnetic anisotropy, which do not prevent magnetic moment alignment in the magnetic field. The  $\text{CoFe}_3\text{O}_4$  sample's remanence ratio, coercivity, and remanent magnetization values are, in order, 0.665, 264.342 Oe, and 43.065 (emu/g). Remanent refers to the magnetization value that remains after the magnetic field is removed [53]. The high coercivity indicates the hard ferromagnetic material that is difficult to demagnetize. Low coercivity formation indicates the formation of soft ferromagnetic and mild magnetism, whereas high coercivity formation indicates the formation of hard ferromagnetic and hard magnetism. The magnetic hysteresis loop of nanomagnetic cadmium ferrite particles demonstrated soft ferromagnetic behavior. Because of its low coercivity and low remanence magnetization, the sample is deemed soft magnetic. This means that it can only withstand low appropriate magnetism and is easily demagnetized. The magneton number of the sample was determined using [47]:

$$n_B = \frac{M_w \times M_s}{5585}, \quad (4)$$

where  $M_s$  is the saturation magnetization and  $M_w$  is the molecular weight. In this research, the particle-particle interaction was studied using coupling constant ( $\lambda$ ). The coupling constant is defined as the ratio of the magnetic dipole interaction energy between two coated particles in contact with each other's thermal energy. It gives information about the strength of the particle-particle interaction as well as an estimate of the typical force used when the nanoparticles interact. The coupling constant was determined using [47]:

$$\lambda = \frac{m^2}{d_h^3 K_B T}, \quad (5)$$

where  $m$  is the particle's mass,  $k_B$  is the Boltzmann constant,  $k$  is the anisotropy constant, and  $T$  is the temperature. The  $\text{CoFe}_3\text{O}_4$  sample forms strong inter-particle interactions because its coupling constant, 1.97, is greater than unity. The  $\text{ZnFe}_3\text{O}_4$  and  $\text{CdFe}_3\text{O}_4$  samples have coupling constants of 1.35 and 0.863, respectively. Only when the coupling constant is

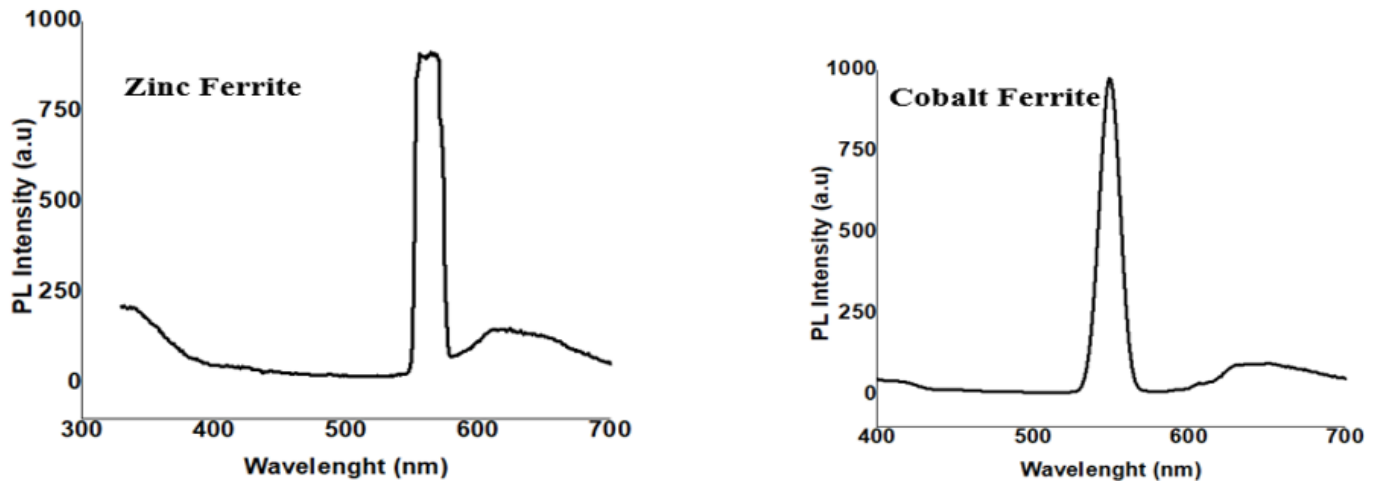


Figure 8. Photoluminescence spectral of (a)  $\text{MFe}_3\text{O}_4$  ( $\text{M} = \text{Zn}^{2+}$ ) magnetic samples, (b)  $\text{MFe}_3\text{O}_4$  ( $\text{M} = \text{Co}^{2+}$ ) magnetic samples

Table 1. Magnetic Parameters of  $\text{MFe}_3\text{O}_4$  ( $\text{M} = \text{Cd}^{2+}, \text{Co}^{2+}, \text{Zn}^{2+}$ ) Magnetic Samples.

Sample	Saturation magnetization $M_s$ (emu/g)	Remanance magnetization $M_r$ (emu/g)	$M_r/2$	Remanant Ratio $M_{r,s} = M_r/M_s$	Coercivity $H_c$ (Oe)	Magnetic anisotropy K ( $\text{MJ}/\text{m}^3$ )	Magneton number $n_B$
$\text{M} = \text{Cd}^{2+}$	24.041	10.654	5.327	0.443	54.654	266.492	1.037
$\text{M} = \text{Co}^{2+}$	64.779	43.065	21.53	0.665	264.342	4877.999	2.186
$\text{M} = \text{Zn}^{2+}$	39.263	25.609	12.81	0.652	128.943	2166.693	1.449

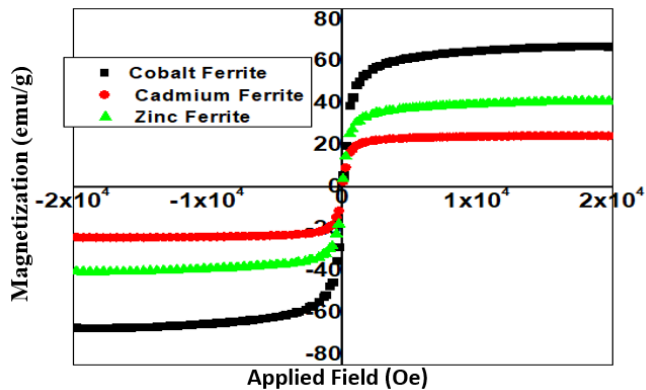


Figure 9. Hysteresis loop of  $\text{MFe}_3\text{O}_4$  ( $\text{M} = \text{Cd}^{2+}, \text{Zn}^{2+}, \text{Co}^{2+}$ ) magnetic sample.

greater than one can the strong chain-like structure overcome the thermal reaction [47]. Due to spin canting effects or surface spin disorder [54], the saturation magnetization of the crystalline cobalt ferrite sample is lower than that of the bulk  $\text{CoFe}_2\text{O}_4$  sample (80 emu/g) [55]. Equation (6) links saturation magnetization to coercive force:

$$H_c = \frac{2k_1}{\mu_0 M_s}. \quad (6)$$

The coercive force is inversely proportional to saturation magnetization, according to equation (6). Ferrite samples with significant saturation magnetization and high equivalent coerciv-

ity up to 600 Oe are suitable for use as longitudinal magnetic recording media [56], according to Li *et al.* [57]. None of the samples are suitable for use as magnetic recording media because all of the coercivity values found in this work are less than 600 Oe.

Research indicates that the size of the synthesized particles' crystallites has an impact on the magnetization. Cobalt ferrite exhibits a higher magnetic effect and has a larger crystallite size of 32.46 nm. The crystallite sizes of zinc and cadmium ferrite are 18.76 nm and 10.54 nm, respectively, and they show magnetization values of 39.263 emu/g and 24.051 emu/g. This outcome showed that the magnetic effect increased as crystallite increased. Ferrite samples with magnetization between 58.32 and 67.32 emu/g and crystallite sizes between 15.7 and 33.5 nm are suitable for use in microwave application, per a 2019 study by Maksoud *et al.* [58]. The cobalt ferrite sample that is currently being synthesized is ferromagnetic [59] and has a magnetization of 64.779 emu/g and crystallite size 32.46 nm, making it suitable for microwave applications. Because their magnetization is less than 58.32 emu/g, other samples, such as zinc ferrite and cadmium ferrite, are not appropriate for this application. The 2021 study by Ali *et al.* [60] states that ferrite samples with crystallite sizes ranging from 10.96 to 14.28 nm and magnetization ranging from 24.20 to 37.16 emu/g are suitable for use in longitudinal magnetic recording media. The cadmium ferrite sample that possesses these qualities is therefore appropriate for use in magnetic recording media. A ferrite sample with a magnetization of 2.722 emu/g and a crystallite size of 250 nm is deemed suitable for use as a humidity sensor, per

Kim *et al.* [61]. None of the synthesized samples can be used as a humidity sensor because none of them show these traits. According to Cambale *et al.* [62], ferrite samples with crystallite sizes between 23.77 and 27.09 nm and magnetization between 52.55 and 68.94 emu/g can be employed as gas sensors. As an alternative, Caltun *et al.* [63] proposed that the material can be utilized as automotive sensors if its crystallite size is between 12.04 and 15.02 nm and its magnetization is between 77 and 96 emu/g.

$$M_{rs} = \frac{M_r}{M_s} \quad (7)$$

In this research, squareness ratio of the synthesized ferrite samples was determined using equation (7) [64]. Synthesized samples display a single magnetic domain structure if the squareness ratio is equal to or larger than 0.5 ( $M_{rs} \geq 0.5$ ), whereas the ferrite sample displays a multi magnetic domain structure if the squareness ratio is less than 0.5 ( $M_{rs} < 0.5$ ), according to the literature [64]. The current synthetic samples (CoFe<sub>3</sub>O<sub>4</sub> and ZnFe<sub>3</sub>O<sub>4</sub>) have a squareness ratio greater than 0.5, indicating that the ferrite samples display a single magnetic domain structure, but CdFe<sub>3</sub>O<sub>4</sub> displays a squareness ratio less than 0.5, indicating that it has a multi-magnetic domain structure. According to the report, synthesized material is hard magnetic and appropriate for applications in high frequency device, if coercivity  $H_c$  is greater than  $\frac{M_r}{2}$ ; on the other hand, if the sample is semi hard magnetic, coercivity  $H_c$  is less than  $\frac{M_r}{2}$ , this makes the material to be suitable for application in information storage device [65]. Since the currently produced magnetic samples show coercivity  $H_c$  greater than  $\frac{M_r}{2}$ , the materials are hard magnetic and appropriate for use in high frequency devices. The synthesized ferrite samples exhibit coercivity  $H_c$  not less than  $\frac{M_r}{2}$ , the samples are henceforth hard magnetic and appropriate in high frequency device application. None of the samples are appropriate for application in information storage device, because their coercivity  $H_c$  does not less than  $\frac{M_r}{2}$ .

$$K = \frac{H_c M_s}{2} \quad (8)$$

Research indicates that magnetic anisotropy, which is reliant on coercivity and saturation magnetization, characterizes the preferred orientation on the spin of a usable magnetic system that does not align with an external magnetic field. The formation of spin disorder at the particle surface caused the anisotropy exchange.  $K = \frac{H_c M_s}{2}$  is used to evaluate the magnetic anisotropy of the ferrite samples [66]. Here,  $k$  stands for magnetic anisotropy,  $H_c$  for coercivity, and  $M_s$  for saturation magnetization. Cobalt ferrite sample exhibits a high magnetic anisotropy while cadmium ferrite exhibits lower magnetic anisotropy. When compared to other ferrite compounds, CoFe<sub>2</sub>O<sub>4</sub> have a number of advantageous and distinctive characteristics, such as strong magnetocrystalline anisotropy, high coercivity ( $H_c$ ), and moderate saturation magnetization ( $M_s$ ). Similar result was reported by Apostolov *et al.* [58] and Rao *et al.* [67].

## 4. Conclusion

CoFe<sub>3</sub>O<sub>4</sub>, ZnFe<sub>3</sub>O<sub>4</sub>, and CdFe<sub>3</sub>O<sub>4</sub> nanomagnetic samples were successfully synthesized by the co-precipitation method. The XRD analysis showed that the ideal orientation for the formation of cubic and single phase spinel is the (311) reflection plane. The samples' crystallite sizes for CdFe<sub>3</sub>O<sub>4</sub>, ZnFe<sub>3</sub>O<sub>4</sub>, and CoFe<sub>3</sub>O<sub>4</sub> are 11.54 nm, 18.76 nm, and 32.63 nm, respectively. Because of its high optical gain, the cobalt ferrite sample exhibits the best optical features, while the cadmium ferrite sample exhibits optical losses. Because of its low optical loss, cobalt ferrite sample is now a fantastic choice for optoelectronics device applications. However, in the cadmium ferrite magnetic samples, greater absorbance was discovered in the UV region. This sample would therefore work better with UV control and detectors in residential systems. Little photo-reflection was produced by the cobalt ferrite magnetic sample, suggesting that the samples would work well as an anti-reflective coating in some engineering equipment where low reflection is needed. The samples are hard magnetic and suitable for use in high frequency device applications because  $H_c > M_r/2$ . Cadmium ferrite exhibits a multi magnetic domain structure, whereas zinc and cobalt ferrite show a single magnetic domain structure, because of a squareness ratio of less than 0.5. The production of high coercivity is a sign that hard ferromagnetic material is developing. The presence of an impurity level in the ferrites lattice causes the emission band shifting. The formation of cyan, green, and yellow light emission is revealed by the shifting of the peaks at 510 nm, 550 nm, and 570 nm from a high energy level to a low energy level.

## References

- [1] A. S. Lanje, R. S. Ningthoujam, S. J. Shrama, R. K. Vatsa & R. B. Pode, "Luminescence properties of Sn<sub>1-x</sub>FexO<sub>2</sub> nanoparticles", International Journal of Nanotechnology 7 (2010) 979. <https://www.inderscienceonline.com/doi/abs/10.1504/IJNT.2010.034703>
- [2] Y. Jiang, S. Decker, C. Mohs & K. J. Klabunde, "Catalytic solid state reactions on the surface of nanoscale metal oxide particles", Journal of Catalysis 180 (1998) 24. <https://www.sciencedirect.com/science/article/abs/pii/S0021951798922576>
- [3] S. Lee, S. U. S. Choi, S. Li & J. A. Eastman, "Measuring thermal conductivity of fluids containing oxide nanoparticles", ASME Journal of Heat Transfer 121 (1999) 280-289. <https://doi.org/10.1115/1.2825978>
- [4] K. B. Modi, P. V. Tanna, S. S. Laghate & H. H. Joshi, "The effect of Zn<sup>+2</sup> substitutions on some structural properties of CuFeCrO<sub>4</sub> system", Journal of Material Science Letter 19 (2000) 1111. <https://link.springer.com/article/10.1023/A:1006784304415>
- [5] O. Silva & P. C. Morais, "Investigation of anisotropy in cadmium ferrite-based ionic magnetic fluid using magnetic resonance", Journal of Magnetism and Magnetic Material 289 (2005) 136. <https://www.sciencedirect.com/science/article/abs/pii/S0304885304012648>
- [6] P. K. Nayak, "Synthesis and characterization of cadmium ferrite", Materials Chemistry and Physics 112 (2008) 24. <https://www.sciencedirect.com/science/article/abs/pii/S0254058408002824>
- [7] M. Yokoyama, E. Ohta, T. Sato & T. Sato, "Magnetic properties of ultrafine particles and bulk material of cadmium ferrite", Journal of Magnetism and Magnetic Material 183 (1998) 173. <https://www.sciencedirect.com/science/article/abs/pii/S0304885397010731>
- [8] G. Albanese, A. Deriu, G. Calestani, F. Leccabue & B. E. Watas, "Formation of cadmium-containing W-type hexagonal ferrite", Journal of Material Science 27 (1992) 6146. <https://link.springer.com/article/10.1007/BF01133764>

- [9] D. Ravinder, S. S Rao & P. Shalini, "Room temperature electric properties of cadmium-substituted nickel ferrites", *Material Letter* **57** (2003) 4040. <https://www.sciencedirect.com/science/article/abs/pii/S0167577X03000892>
- [10] S. S Bellad, S. C Watawe, A. M Shaikh & B. K Chougule, "Cadmium substituted high permeability lithium ferrite", *Bulleting of Material Science* **232** (2000) 83. <https://link.springer.com/article/10.1007/bf02706546>
- [11] M. ul-Islam, T. Abass & M. A Chaudhry, "Electrical properties of Cd-substituted copper ferrite", *Material letters* **53** (2000) 30. <https://www.sciencedirect.com/science/article/abs/pii/S0167577X01004487>
- [12] B. Gillot, D. Thiebaut, M. Laarj & T. Thermochem, "Synthesis of stoichiometric cadmium substituted magnetites and formation by oxidation of solid solutions of cadmium ferrite and  $\gamma$ -iron oxide", *Thermochemica Acta* **342** (1999) 167. <https://www.sciencedirect.com/science/article/abs/pii/S004060319900310X>
- [13] M. B Shelar, P. A Jadhav, S. S Chougule, M. M Mallapur & B. K Chougule, "Structural and electrical properties of nickel cadmium ferrites prepared through self-propagating auto combustion method", *Journal of Alloys and Compounds* **476** (2009) 760. <https://www.sciencedirect.com/science/article/abs/pii/S0925838808015648>
- [14] B. Viswanathan & V. R. K. Murthy, *Ferrite Materials: science and technology*, Narosa Publications (1990). <https://search.worldcat.org/title/ferrite-materials-science-and-technology/oclc/23290304>
- [15] M. Srivastava, A. K Ojha, S. Chaubey & A. Materny, "Synthesis and optical characterization of nanocrystalline  $\text{NiFe}_2\text{O}_4$  structures", *Journal of Alloy Compound* **481** (2009) 515. <https://doi.org/10.1016/j.jallcom.2009.03.027>
- [16] H. W. Cheng, J. Luo & C. J. Zhong, "SERS nanoprobe for bio-application", *Frontier of Chemical Science and Engineering* **9** (2015) 428. <https://doi.org/10.1007/s11705-015-1536-0>
- [17] K. C. Mouli, T. Joseph & K. Ramam, "Synthesis and magnetic studies of Co-Ni-Zn ferrite nano crystals", *Journal of Nanoscience and Nanotechnology* **9** (2009) 5596. <https://www.ingentaconnect.com/contentone/asp/jnn/2009/00000009/00000009/art00088>
- [18] M. Das & D. Chakraborty, "Influence of alkali treatment on the fine structure and morphology of bamboo fibers", *Journal of Applied Polymer Science* **102** (2006) 505. <https://doi.org/10.1002/app.25115>
- [19] D. De & B Adhikari, "Reclaiming of rubber by a renewable material (RRM)", *Journal of Applied Polymer Science* **42** (2000) 1493. [https://doi.org/10.1002/\(SICI\)1097-4628\(20000321\)75:12<1493::AID-APP8>3.0.CO;2-U](https://doi.org/10.1002/(SICI)1097-4628(20000321)75:12<1493::AID-APP8>3.0.CO;2-U)
- [20] R. Lebourgeois & C. Coillot, "Mn-Zn ferrites for magnetic sensor in space applications", *Journal of Applied Physics* **103** (2008) 07E510. <https://doi.org/10.1063/1.2838994>
- [21] A. K. Hossain, T. S. Biswas, T. Yanagida, H. Tanaka, H. Tabata & T. Kawai, "Enhancement of microstructure and initial permeability due to Cu substitution in  $\text{Ni}_{0.50-x}\text{Cu}_x\text{Zn}_{0.50}\text{Fe}_2\text{O}_4$  ferrites", *Material Chemistry and Physics* **120** (2010) 461. <https://doi.org/10.1016/j.jmmm.2011.02.031>
- [22] S. J Yagmour, M. Hafez, K. Ali & W. Elshirbeeny, "The influence of zinc ferrites nanoparticles on the thermal, mechanical, and magnetic properties of rubber nanocomposites Polymer Composites", **4** (2012) 1672. <https://doi.org/10.1002/pc.22300>
- [23] V. G. Harris, A. Geiler, Y. J. Chen, S. D. Yoon, M. Z. Wu, A. Yang, Z. H. Chen, P. He, P. V. Parimi, X. Zuo, C. E. Patton, M. Abe, O. Acher & C. Vittoria, "Recent advances in processing and applications of microwave ferrites", *Journal of Magnetism and Magnetic Material* **321** (2019) 2035. <https://doi.org/10.1016/j.jmmm.2009.01.004>
- [24] J. D. Adam, L. E. Davis, G. F. Dionne, E. F. Schloemann & S. N. Stitzer, "Ferrite devices and materials", *IEEE. Trans. Microwave Theory Technology* **50** (2002) 721. <https://doi.org/10.1109/22.989957>
- [25] J. S. Bettinger, R. V. Chopdekar, M. Liberati, J. R. Neulinger, M. Zhshiev & Y. Akamwa, "Magnetism and transport of  $\text{CuCr}_2\text{Se}_4$  thin film", *Journal of Magnetism and Magnetic Material*, **318** (2007) 65. <https://doi.org/10.1016/j.jmmm.2007.04.024>
- [26] Y. Suzuki, R. B. Van Dover, E. M. Gyorgy, J. M. Philips, J. Korenivski, J. Werder, C. H Chen, R. J. Cava, R. J. W. F. jewski Peck & K. B. Do, "Structure and magnetic properties of epitaxial spinel ferrite thin film", *Applied Physics Letter* **68** (1996) 714. <https://doi.org/10.1063/1.1063/1.116601>
- [27] E. Pervaiz & I. H. Gul, "Influence of rare earth ( $\text{Gd}^{3+}$ ) on structural, gigahertz dielectric and magnetic studies of cobalt ferrite", *Journal of Physics: Conference series* **439** (2013) 012015. <https://doi.org/10.1088/1742-6596/439/1/012015>
- [28] Y. Kitamoto, S. Kantake, A. Shirasaki, F. Abe & M. Naoe, "Low-temperature fabrication of Co ferrite thin films with high coercivity for perpendicular recording disks by wet process", *Journal of Applied Physics* **85** (1999) 4708. [https://doi.org/10.1016/S0304-8853\(98\)00409-0](https://doi.org/10.1016/S0304-8853(98)00409-0)
- [29] W. F. J. Fontijn, P. J. vander Zaag, L. F. Feiner, R. Metselaar & M. C. A. Devillers, "A consistent interpretation of the magneto-optical spectra of spinel type ferrites", *Journal of Applied Physics*. **85** (1999) 5100. <https://doi.org/10.1063/1.369091>
- [30] C. N. Chinnasamy, A. Narayanasamy, N. Ponpandian, K. Chattopadhyay, H. Guerault & J. M. Greneche, "Magnetic properties of nanostructured ferrimagnetic zinc ferrite", *Journal of physics: Condensed Matter* **12** (2020) 7795. <https://doi.org/10.1088/0953-8984/12/35/314>
- [31] K. A. Manish, S. Anjna, K. M. Indresh, T. Alpna & K. Sunil, "Synthesis of ultra small iron oxide and doped iron oxide nanostructures and their antimicrobial activities", *Journal of Taibah University for Science* **13** (2019) 280. <https://doi.org/10.1080/16583655.2019.1565437>
- [32] S. Saleem, M. N Ashiq, S. Manzoor, U. Ali, R. Liaqat, A. Algahtani, S. Mujtaba, V. Tirth, A. M. Alsuhaibani, M. S. Refat, A. Ali, M. Aslam & A. Zaman, "Analysis and characterization of opto-electronic properties of iron oxide ( $\text{Fe}_2\text{O}_3$ ) with transition metals (Co, Ni) for the use in the photodetector application", *Journal of materials research and technology* **25** (2023) 6150. <https://doi.org/10.1016/j.jmrt.2023.07.065>
- [33] S. Arshad, A. Hussain, S. Noreen, N. Bibi, M. B. Tahir, J. Rehman, M. Jabeen, H. Benish Munawar & S. Rahman, "Structural, mechanical, electrochemical and optical properties of  $\text{MFe}_2\text{O}_4$  (M=Zn, Cu, Si) ferrites for electrochemical, photocatalytic and optoelectronic applications", *Journal of Solid State Chemistry* **330** (2024) 124504. <https://doi.org/10.1016/j.jssc.2023.124504>
- [34] H. B. Desai & A. R. Tanna, "Effect of substitution on the electric and magnetic properties of ferrites: Ferrites and Multiferroics", *Engineering Materials Springer Singapore* (2021) 49. [https://doi.org/10.1007/978-981-16-7454-9\\_3](https://doi.org/10.1007/978-981-16-7454-9_3)
- [35] V. V. Jadhav, S. D. Shirsat, U. B. Tumberphale & R. S. Mane, "Spinel ferrite nanostructures for energy storage devices in micro and nano technologies", *Elsevier Netherland* (2020) 35. <https://doi.org/10.1016/B978-0-12-819237-5.00003-1>
- [36] S. Thakur, N. Sharma, A. Varkia & J. Kumar, "Structural and optical properties of copper doped ZnO nanoparticles and thin films", *Advances in Applied Science Research* **5** (2014) 18. [https://doi.org/10.1016/S0022-2313\(99\)00599-2](https://doi.org/10.1016/S0022-2313(99)00599-2)
- [37] M. D. Tyona, S. B. Jambure, C. D. Lokhande, A. G. Banpurkar & R. U. Osuji, "Dye-sensitized solar cells based on Al-doped ZnO photoelectrodes sensitized with rhodamine", *Materials Letters* **220** (2018) 281. <https://doi.org/10.1016/j.matlet.2018.03.040>
- [38] S. C. Suman, A. Kumar & P. Kumar, "Zn Doped  $\alpha$ - $\text{Fe}_2\text{O}_3$ : An efficient material for UV driven photocatalysis and electrical conductivity", *Crystals* **10** (2020) 273. <https://doi.org/10.3390/cryst10040273>
- [39] N. Kislov, S. Srinivasan, U. Emirov & E.K. "Stefanakis", "Optical absorption, red and blue shifts in  $\text{ZnFe}_2\text{O}_4$  nanoparticles", *Materials Science and Engineering B*, **153** (2008) 70. <https://doi.org/10.1016/j.mseb.2008.10.032>
- [40] P. P. Hankare, R. P. Patil, A. V. Jadhav, R. S. Pandav, K. M. Garadkar, R. Sasikala & A. K. Tripathi, "Synthesis and characterization of nanocrystalline Ti- substituted Zn ferrite", *Journal of Alloys Compound* **509** (2011) 2160. <https://www.sciencedirect.com/science/article/abs/pii/S0925838810027039>
- [41] P. Thakur, K. Gupta, P. Thakur, A. S. Kumar, V. Sudarsanan, P. Sharma & M. Lal, "Improvement in the structural, dielectric, and magnetic properties of CFO-doped KNNS-BKT ceramics". *Journal of Material Science: Mater Electron* **34** (2023) 311. <https://doi.org/10.1007/s10854-022-09782-6>
- [42] B. H Devmunde, P. S Bhalerao & M. B Solunke, "Structural morphological and infrared properties of  $\text{Cd}^{2+}$  substitutes Nickel ferrite particles", *Journal of Physics: Conference Series* **1644** (2020) 012021. <https://iopscience.iop.org/article/10.1088/1742-6596/1644/1/012021/meta>
- [43] S. Sagadevan, Z. C. Zaira & F. Rahman, "Preparation and characterization of Nickel ferrite nanoparticles via co-precipitation method", *Material Research* **21** (2018) 2016. <https://doi.org/10.1590/1980-5373-MR-2016-0533>

- [44] D. Ahmad, N. Mehboob, A. Zaman, N. Ahmed, M. Mushtaq, K. Althubeiti, A. Ali, F. Sulitana & K. Bashir, "Synthesis and characterization of Ce<sup>3+</sup>-doped Ni<sub>0.5</sub>Cd<sub>0.5</sub>Fe<sub>2</sub>O<sub>4</sub> nanoparticles by Sol-gel: Auto-combustion method", *Coatings* **11** (2021) 1156. <https://doi.org/10.3390/coatings11101156>
- [45] D. Manojite, A. Mukherjee & S. T. Hari, "Characterization of cadmium substituted nickel ferrites prepared using auto-combustion technique", *Processing and Application of Ceramics* **9** (2015) 193. <https://doiserbia.nb.rs/Article.aspx?id=1820-61311504193D>
- [46] A. A. Ibiyemi, G. T. Yusuf & A. Olusola, "Influence of temperature and magnetic field on rheological behavior of ultra-sonicated and oleic acid coated cobalt ferrite ferrofluid", *Physica scripta* **96** (2021) 125842. <https://doi.org/10.1088/1402-4896/ac2ecb>
- [47] C. Mahesh, A. Shankar, N. Jahan, K. Jain & R. P. Pant, "Improved properties of bidispersed magnetorheological fluids", *Royal Society of Chemistry Advance* **4** (2014) 53960. <https://doi.org/10.1039/C4RA07431A>
- [48] A. A. Ibiyemi, "Characteristics of temperature-dependent shear flow in an ultrasonicated ferrofluid", *Recent Advances in Natural Sciences* **1** (2023) 28. <https://doi.org/10.61298/rans.2023.1.2.28>
- [49] A. A. Ibiyemi, M. A. Ilyas & J. Lawal, "Annealing effect on morphology, surface roughness and structure of thermally evaporated tin oxide thin films", *Recent Advances in Natural Sciences* **1** (2023) 38. <https://doi.org/10.61298/rans.2023.1.2.38>
- [50] S. Thakur, N. Sharma, A. Varkia & J. Kumar, "Structural and optical properties of copper doped ZnO nanoparticles and thin films", *Advances in Applied Science Research* **5** (2014) 18. [https://www.researchgate.net/publication/264634814\\_Structural\\_and\\_optical\\_properties\\_of\\_copper\\_doped\\_ZnO\\_nanoparticles\\_and\\_thin\\_films](https://www.researchgate.net/publication/264634814_Structural_and_optical_properties_of_copper_doped_ZnO_nanoparticles_and_thin_films)
- [51] A. V. Dijken, E.A. Meulenkaamp, D. V. Ibergh & A. Meijerink, "Identification of the transition responsible for the visible emission in ZnO using quantum size effects", *Journal of Luminescence* **90** (2000) 123. [https://doi.org/10.1016/S0022-2313\(99\)00599-2](https://doi.org/10.1016/S0022-2313(99)00599-2)
- [52] S. Suwanboon, T. Ratana & W. T. Ratana, "Effect of Al and Mn Dopant on structural and optical properties of ZnO thin film prepared by Sol-gel route", *Journal of Science and Technology* **4** (2007) 111. <https://wjst.wu.ac.th/index.php/wjst/article/view/129>
- [53] M. B. Islam, M. R. Pavel, M. R. Islam & M. J. Haque, "Synthesis of Cobalt Ferrite Nanoparticles using microemulsion method: structure, morphology, and magnetic properties", *Journal of Engineering Science* **13** (2022) 81. <https://doi.org/10.3329/jes.v13i1.60565>
- [54] X. H. Li, C. L. Xu, X. H. Han, L. Qiao, T. Wang & F. S. Li, "Synthesis and Magnetic Properties of Nearly Monodisperse CoFe<sub>2</sub>O<sub>4</sub> nanoparticles through a simple hydrothermal condition", *Nanoscale Research Letter* **5** (2010) 1039. <https://doi.org/10.1007/s11671-010-9599-9>
- [55] A. A. Ibiyemi & G. T. Yusuf, "Rheological investigation of strain rate and magnetic field on the magnetorheology of zinc ferrite ferrofluid", *Applied Physics A* **128** (2022) 591. <https://link.springer.com/article/10.1007/s00339-022-05720-9>
- [56] Q. Lin, J. Xu, F. Yang, J. Lin, H. Yang & Y. He, "Magnetic and mossbauer spectroscopy studies of zinc-substituted cobalt ferrites prepared by the sol-gel method", *Materials (Basel)* **11** (2018) 1799. <https://www.mdpi.com/1996-1944/11/10/1799>
- [57] Y. Li, R. Liu, Z. Zhang & C. Xiong, "Synthesis and characterization of nanocrystalline BaFe<sub>9.6</sub>Co<sub>0.8</sub>Ti<sub>0.8</sub>Mn<sub>0.8</sub>O<sub>19</sub> particles", *Materials Chemistry and Physics* **64** (2013) 256. <https://www.sciencedirect.com/science/article/abs/pii/S0254058499002187>
- [58] A. Apostolov, I. Apostolova & J. Wesselinowa, "Specific absorption rate in Zn-doped ferrites for self-controlled magnetic hyperthermia", *The European Physical Journal B* **92** (2019) 3. <https://doi.org/10.1140/epjb/e2019-90567-2>
- [59] P. Thakur, K. Kishore, M. Singh, S. Sharma, P. Sharma, P. Sharma & M. Lal, "Structural, morphological, and magnetic properties of CoFe<sub>2</sub>O<sub>4</sub> nano-ferrites synthesized via co-precipitation route", *Materials Today: Proceedings* 2023. <https://doi.org/10.1016/j.matpr.2022.12.233>
- [60] M. I. A. Abdel Maksoud, A. El-ghandour, G. S. El-Sayyad, A. S. Awed, A. H. Ashour, A. I. El-Batal, M. Gobara, E. K. Abdel-Khalek & M. M. El-Okri, "Incorporation of Mn<sup>2+</sup> into cobalt ferrite via sol-gel method: insights on induced changes in the structural, thermal, dielectric, and magnetic properties", *Journal of Sol-gel Science and Technology* **90** (2019) 631. <https://doi.org/10.1007/s10971-019-04964-x>
- [61] C. H. Kim, Y. Myung, Y. J. Cho, H. S. Kim, S. -H. Park, J. Park, J. -Y. Kim & B. Kim, "Electronic structure of vertically aligned Mn-doped CoFe<sub>2</sub>O<sub>4</sub> nanowires and their application as humidity sensors and photodetectors", *Journal of Physics and Chemistry C* **113** (2009) 7085. <https://pubs.acs.org/doi/abs/10.1021/jp900165c>
- [62] R. C. Kambale, P. A. Shaikh, N. S. Harale, V.A. Bilur, Y. D. Kolekar, C. H. Bhosale & K. Y. Rajpure, "Structural and magnetic properties of Co<sub>1-x</sub>Mn<sub>x</sub>Fe<sub>2</sub>O<sub>4</sub> spinel ferrites synthesized by combustion route", *Journal of Alloys Compound* **490** (2010) 568. <https://www.sciencedirect.com/science/article/abs/pii/S0925838809020581>
- [63] O. Caltun, G. S. N. Rao, K. H. Rao, B. R. Parvatheeswara, I. Dumitru, C. -O. Kim & C. Kim, "The influence of Mn doping level on magnetostriction coefficient of cobalt ferrite", *Journal of Magnetism and Magnetic Material* **316** (2007) 618. <https://doi.org/10.1016/J.JMMM.2007.03.045>
- [64] S. Dabagh, A. A. Ati, R. M. Rosnan, S. Zare & Z. Othaman, "Effect of Cu-Al substitution on the structural and magnetic properties of Co ferrites", *Material Science: Semiconductor Process* **33** (2015) 1. <https://doi.org/10.1016/J.MSSP.2015.01.025>
- [65] M. N. Ashiq, R. B. Qureshi, M. A. Malana & M. Ehsan, "Fabrication, structural, dielectric and magnetic properties of tantalum and potassium doped M-type strontium calcium hexaferrites", *Journal of Alloy Compound* **651** (2015) 266. <https://doi.org/10.1016/j.jallcom.2015.05.181>
- [66] A. A. Ibiyemi, G. T. Yusuf, O. Olubosede, A. Olusola & H. A. Akande, "Photoelectric and magnetic properties of chemically synthesized Cd-Ni Ferrite nanomagnetic particles", *Physica Scripta* **97** (2022) 025804. <https://doi.org/10.1088/1402-4896/ac4a95>
- [67] A. P. Rao, S. K. Rao, T. R. K. PydiRaju, G. Kapusetti, M. Choppadandi, M. C. Varma & K. H. Rao, "A systematic study of cobalt-zinc ferrite nanoparticles for self-regulated magnetic hyperthermia", *Journal of Alloys Compound* **794** (2019) 60. <https://doi.org/10.1016/j.jallcom.2019.04.242>